
REx: Data-Free Residual Quantization Error Expansion

Edouard Yvinec^{1,2}Arnaud Dapogny²Matthieu Cord^{2,3}Kevin Bailly^{1,2}¹ Sorbonne Université, CNRS, ISIR, f-75005, 4 Place Jussieu 75005 Paris, France² Datakalab, 114 boulevard Malesherbes, 75017 Paris, France³ Valeo, 100 rue de Courcelles, 75017 Paris, France

ey@datakalab.com

Abstract

Deep neural networks (DNNs) are nowadays ubiquitous in the computer vision landscape. However, they suffer from high computational costs in inference, particularly when evaluated on edge devices. This problem is generally addressed *via* post-hoc quantization, *i.e.* converting the DNN values (weights and inputs) from floating point into e.g. int8, int4 or ternary quantization. In this paper, we propose REx, a data-free quantization algorithm for pre-trained models that is compliant with data protection regulations, convenient and fast to execute. First, we improve upon the naive linear quantization operator by decomposing the weights as an expansion of residual quantization errors. Second, we propose a budgeted group-sparsity formulation to achieve better accuracy vs. number of bit-wise operation trade-offs with sparse, higher expansion orders. Third, we show that this sparse expansion can be approximated by an ensemble of quantized neural networks to dramatically improve the evaluation speed through more efficient parallelization. We provide theoretical guarantees of the efficiency of REx as well as a thorough empirical validation on several popular DNN architectures applied to multiple computer vision problems, e.g. ImageNet classification, object detection as well as semantic segmentation. In particular, we show that REx significantly outperforms existing state-of-the-art data-free quantization techniques.

1 Introduction

Deep neural networks (DNN) achieve outstanding performance on several challenging computer vision tasks such as image classification [19], object detection [25] and semantic segmentation [5]. However, their efficiency comes at a high computational inference cost which limits their deployment, moreso on edge devices when real-time treatment is a concern. This problem can be tackled *via* DNN quantization, *i.e.* by reducing the bit-width representation of the computations from floating point operations to e.g. int8 (8-bits integer representation), int4, int3 or even lower-bit representation such as ternary (where weights values are either -1 , 0 or $+1$) quantization. Because DNN inference principally rely on matrix multiplication, such quantization dramatically diminishes the number of bit-wise operations (as defined in [22]), thus limiting the DNN latency. However, DNN quantization usually comes at the expense of the network accuracy. As a consequence, DNN quantization is an active field of research [11, 39, 20, 1, 26, 34, 37, 44] that aims at limiting this accuracy drop while reducing the number of bit-wise operations.

All the aforementioned methods are data-driven as they either involve training a network from scratch or fine-tune an already trained and quantized one. However, while such approaches usually

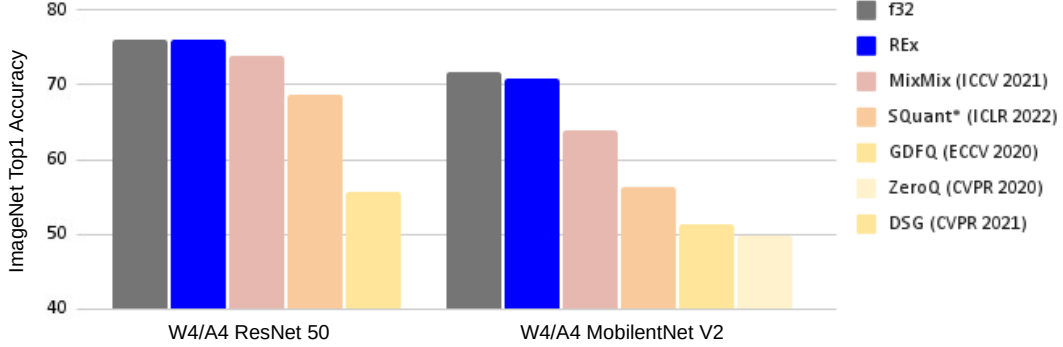


Figure 1: Comparison between the proposed REx quantization method and other state-of-the-art approaches on ImageNet for int4 weights and activations quantization of ResNet 50 and Mobilenet V2. We observe that REx significantly outperforms methods that improve the quantization operation such as SQuant [9] (* using our implementations on Mobilenet V2) as well as methods relying on computationally expensive synthetic data generation such as ZeroQ [4], DSG [41], GDFQ [40] and MixMix [23].

allow lower quantization errors using low bit-wise representations, due to the growing concerns on privacy rights and data privacy, there are a number of real-case scenarios (e.g. health and military services) where data access may be sensible or not available for quantization purposes. Motivated by these observations, several data-free quantization algorithms were published in the recent years [29, 28, 42, 4, 41, 9]: however, these approaches still struggle to narrow the gap with data-driven quantization methods especially on low bit-width, *i.e.* int3 or ternary representation.

The difficulty to reduce quantization error arises from the use of a single value to represent the compressed values. To tackle this issue, we propose to add the residual error of quantization to the quantized model. The residual errors are recursively computed from the original model and the already computed residual errors which shows similarities with the wavelets-based methods for image compression [31, 27].

In this paper, we propose REx, a data-free quantization method standing for **R**esidual errors **E**xpansion. In REx, the weights of each layer are decomposed as an expansion of residual quantization errors: each residue is computed using all the previous residues and the original weights. Furthermore, we propose a budgeted version of this expansion; intuitively, this amounts to put more emphasis on neurons with higher residual errors, thus strictly improving the accuracy. Using this formulation, we show that we can achieve better accuracy trade-offs with sparse, higher expansion orders, given a fixed bit-wise operations budget. Last but not least, we show that a developed network can be approximated by an equivalent ensemble of quantized DNNs. The resulting quantized ensemble achieves outstanding accuracy even in low bit representations (int4) as demonstrated in Fig 1, especially when compared to other recent data-free quantization methods. To sum it up, our contributions are:

- We introduce a novel per-layer, data-free quantization scheme that consists in an expansion as a sum of quantized residual errors. The resulting weight series converge exponentially fast to the original network weights w.r.t. the order of the expansion.
- We introduce a group-sparse expansion with mathematical guarantees on the preservation of the exponential convergence. Given a fixed budget of bit-wise operations, this allows to achieve better trade-offs between accuracy and computational overhead using higher order expansions.
- We show that we can approximate this expansion using ensembles of quantized predictors without changing the budget. Such ensembles allow for an easier parallelization of the overhead computations.

Furthermore, we show through a thorough empirical validation that REx significantly outperforms every state-of-the-art data-free quantization technique. In particular, REx achieves outstanding performances on both standard and low bit range quantization on various DNN architectures applied to ImageNet classification, object detection as well as semantic segmentation.

2 Related Work

2.1 Quantization

In this section, we review existing methods for DNN quantization, with an emphasis on approaches geared towards run-time acceleration rather than memory footprint reduction (e.g. methods that only quantize weights [8, 16, 18, 43]). The vast majority of DNN quantization techniques rely on data usage. Such data-driven approaches can be classified in two main categories. First, methods that involve training a model from scratch [39, 20, 1, 26, 34, 37, 44] usually rely on defining a discrete version of stochastic gradient descent training, typically making use of two distinct models during training: one model with floating-point weight values and a standard training protocol, and a second model with quantized weight updates derived from the first model. Remarkably, Courbariaux et al [11] pushed such quantization methods to deal with very low-bit representation by training Binary Neural Networks, essentially on toy tasks. Another class of data-driven methods [18, 43] rely on fine-tuning a previously trained and quantized DNN. For instance, authors in [43] propose to progressively freeze and quantize a portion of the weights while training the remaining floating-point ones. Oh *et al.* [30] minimize the residual error during training, regarding quantization as some sort of regularization. This method is similar with REx insofar as it uses a second order expansion of the quantization errors. However, it discards the quantization error after training while we propose to keep full, higher order expansions with group-sparse and ensemble formulations to further accelerate the quantized expansions.

2.2 Data-Free Quantization

Nagel et al. [29] discuss the necessity to have data available so as to successfully design a quantization pipeline. The proposed method consists in balancing the weight ranges over the different layers of a model, using scale invariance properties (similarly to [35]) that are specific to piece-wise affine (e.g. ReLU) activation functions, and relying on a traditional, naive quantization operator [22]. The authors note that the magnitude of the quantization error strongly varies with the DNN architecture: as such, already compact architectures such as MobileNets [33] appear as challenging for data-free quantization purposes (for instance, authors in [22] report a dramatic drop to chance-level accuracy without fine-tuning). Lin *et al.* [24] studied the properties of the noise induced by the quantization operator. These properties were later used in SQNR [28], a method that consists in assigning, for each layer, an optimal bit-width representation. Overall, data-free approaches generally struggle to deal with low-bit representation problem, *i.e.* performing quantization into bit widths lower than int4 (e.g. int3 or ternary quantization). However, the proposed method successfully addresses this challenge with the addition of the residual errors in higher order expansions. Furthermore, to compensate for the increased latency, we propose a budgeted expansion as well as a rewriting of the quantized expansion as ensembles for further parallelization.

2.3 Ensemble Methods

Ensemble methods [13] are ubiquitous and widely studied models in the machine learning community, where weak, yet complimentary predictors are aggregated *via* e.g. bagging [2], boosting [15] or gradient boosting [3], to achieve superior performance. Leveraging deep learning and ensemble methods crossovers is still an overlooked subject, partly because standalone DNNs are usually quite robust on their own, and because DNNs already involve a high computational burden. Nevertheless, some methods [32, 17, 36] leveraged deep ensembles to great success for various applications. Of particular interest is the work of Zhu *et al.* [45] which consists in learning ensembles of binary neural networks (BNNs) to reach interesting accuracy vs. inference speed trade-offs, thanks to the potential weakness of predictors working with very low-bit representations such as BNNs, the potential complementarity between these, as well as the fact that, intrinsically, ensembles can be easily parallelised in practice. Our method offers several advantages over [45]: First, REx is applied to existing DNNs in a data-free manner, thus can be applied to accelerate already performing networks without bells and whistles. More importantly, accuracy of the BNN ensembles is significantly lower than that of the original full-precision model, while REx achieves high acceleration without significant accuracy loss. In addition, results reported in [45] are admittedly unstable as the ensembles grow, which the authors attribute to overfitting. REx, however, is robust to such problems as we demonstrate a convergence to the original accuracy with respect to the order of expansion.

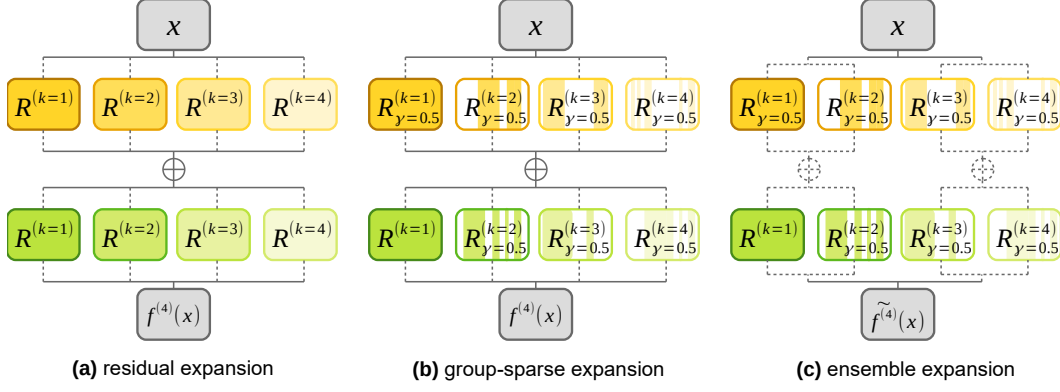


Figure 2: Illustration of the proposed method for a two-layers neural network. **(a)** residual expansion at order 4: the intensity of the colormap indicates the magnitude of the residual error. **(b)** group-sparse expansion for orders $k \geq 1$ ($\gamma = 50\%$ sparsity). **(c)** ensemble expansion with two predictors. Dashed lines indicate parallel computations.

3 Methodology

Fig. 2 illustrates the proposed REx approach. For each layer, the weights are decomposed as an expansion of residual quantization errors ((a)-Section 3.1). Furthermore, we propose a group-sparse formulation to achieve better performance trade-offs given a bit-wise operations budget ((b)-Section 3.2). Last but not least, we show how a developed network can be approximated by an equivalent ensemble ((c)-Section 3.3) allowing easier parallelization (dashed lines on Fig. 2-c).

Let's consider f a trained network with L layers and trained weights W_l (summary of notations in Appendix A). We note Q the b -bits quantization operator that quantizes the weights W_l from $[\min\{W_l\}; \max\{W_l\}] \subset \mathbb{R}$ to $I_q = [-2^{b-1}; 2^{b-1}-1] \cap \mathbb{Z}$ and W_l^q the quantized weights. Classically, this operator is applied separately to each layer and row of the weight matrices: for simplicity, we drop the l notation, and note $(W)_i$ the i^{th} row of W (i.e. the i^{th} neuron of the considered layer). We have:

$$(W^q)_i = Q((W)_i) = \left\lfloor \frac{(W)_i}{(\lambda)_i} \right\rfloor \quad (1)$$

where $\lfloor \cdot \rfloor$ denotes the rounding operation and $(\lambda)_i$ is a row-wise rescaling factor selected such that each coordinate of $(W^q)_i$ falls in I_q , i.e. $(\lambda)_i$ is the maximum between $\frac{|\min\{(W)_i\}|}{2^{b-1}}$ and $\frac{|\max\{(W)_i\}|}{2^{b-1}-1}$. To preserve the network dynamics we define the inverse quantization operator as $Q^{-1}((W^q)_i) = (\lambda)_i (W^q)_i$. The quantized layer is then defined as $f_q : x \mapsto \sigma(Q^{-1}(Q(W)Q(x)) + b)$ where σ is the activation function and b the bias and $Q(x)$ is the quantization of the input x giving rise to a rescaling factor denoted λ_x . Thus, the matrix product $Q(W)Q(x)$ can be computed using lower bit-wise representations. However, strictly speaking, $Q^{-1}((W^q)_i) \neq (W)_i$. One solution to this problem is to leverage the error residue.

3.1 Residual Quantization

The residual error is $W - Q^{-1}(W^q)$. Let $R^{(1)} = W^q$ and $R^{(K)}$ be the K^{th} residual expansion term such that:

$$R^{(K)} = Q \left(W - \sum_{k=1}^{K-1} Q^{-1}(R^{(k)}) \right) \quad (2)$$

The $R^{(K)}$ corresponds to the residual error from $(W - Q^{-1}(\sum_{k=1}^{K-1} R^{(k)}))$. This allows us to define $f^{(K)}$ the expansion as a sum of quantized residual errors

$$f^{(K)} : x \mapsto \sigma \left(\sum_{k=1}^K R^{(k)} Q(x) \lambda_{R^{(k)}} \lambda_x + b \right) \quad (3)$$

where λ_a is the rescaling factor corresponding to the quantization of a (e.g. λ_x and $\lambda_{R^{(k)}}$ correspond to the rescaling of input x and $R^{(k)}$, respectively). The maximum error between the de-quantized and original weights decreases exponentially w.r.t. the expansion order. Formally:

Lemma 1. *Let f be a layer with weights $W \in \mathbb{R}^n$ with a symmetric distribution. We denote $R^{(k)}$ the k^{th} quantized weight from the corresponding residual error. Then the error between the rescaled $W^{(K)} = Q^{-1}(R^{(K)})$ and original weights W decreases exponentially, i.e.:*

$$\left| w - \sum_{k=1}^K w^{(k)} \right| \leq \left(\frac{1}{2^{b-1} - 1} \right)^{K-1} \frac{(\lambda_{R^{(K)}})_i}{2} \quad (4)$$

where w and $w^{(k)}$ denote the elements of W and $W^{(k)}$ and $(\lambda_{R^{(k)}})_i$ denotes the row-wise rescaling factor at order k corresponding to w , as defined in equation 1.

We provide proof of this result in Appendix B.1. This implies that, in practice, a network can be quantized with high fidelity with only a few orders. In what follow, we propose a group-sparse formulation to achieve better performance trade-offs given a fixed budget.

3.2 Group-Sparsity for Budgeted Expansion

Let $\gamma \in]0, 1]$ denote a threshold parameter that defines, for the whole network, the proportion of channels to develop. Let K be the order of the expansion and $\beta = (K - 1)\gamma$ the budget in terms of bit-wise operations.

Inter-layer budgeting: we split the budget over the layers by defining layer-wise thresholds γ^l such that $\sum_l |W_l| \gamma^l = \gamma \sum_l |W_l|$ where $|W_l|$ denotes the number of scalar parameters in layer l . The best tested strategy is a linear ascending function of l , i.e. $\gamma^l = al + \gamma^1$, $a > 0$:

$$\begin{cases} a = \frac{(1-\gamma) \sum_l |W_l|}{\sum_l l |W_l| - \sum_l |W_l|} \\ \gamma^1 = 1 - aL \\ \gamma^l = \text{clip}_0^1(al + \gamma^1) \end{cases} \quad (5)$$

with clip_0^1 is the clipping operator of bounds 0 and 1. This strategy gives more budget to the last layers which correspond to the largest layers. We validate this strategy several options for setting the (γ^l) from γ (see Appendix C for more details).

Intra-layer budgeting: Let $N_i^{(k)}$ denotes the L_1 norm of an output channel i of the k -th order residue $R^{(k)}$. The sparse residue is defined as:

$$\left(R_\gamma^{(k)} \right)_i = (R^{(k)})_i \cdot \mathbb{1}_\gamma^{(k)} \quad (6)$$

where \cdot is the element-wise multiplication, $\mathbb{1}_\gamma^{(k)} = \mathbb{1}_{\{N_i^{(k)} \geq \tau_\gamma^{(k)}\}}$ and $\tau_\gamma^{(k)}$ is a threshold defined as the γ percentile of $N^{(k)}$. In other words, we remove a proportion γ of channels from residue $R^{(k)}$ that are the least important, as indicated by their norm $N^{(k)}$. Note however that these pruned channels can be encoded in subsequent residuals, i.e. $R^{(k')}$, with $k' > k$. The result from Lemma 1 becomes:

Lemma 2. *Let f be a layer of real-valued weights W with a symmetric distribution. Then we have*

$$\left| w - \left(\sum_{k=1}^{K-1} w^{(k)} + Q^{-1} \left(R_\gamma^{(K)} \right) \right) \right| \leq \frac{\left\| N^{(K)} \cdot \mathbb{1}_\gamma^{(K)} \right\|_\infty (\lambda_{R^{(K)}})_i}{(2^{b-1} - 1)^K 2} \quad (7)$$

where $\|\cdot\|_\infty$ is the infinite norm operator with the convention that $\|0\|_\infty = 1$ and $(\lambda_{R^{(k)}})_i$ denotes the row-wise rescaling factor at order K corresponding to w .

In other words, the the group-sparse expansion preserves the exponential convergence property (see Appendix B.2 for proof of this result). Using this sparse version of REx we can adjust the number of computations to suit a budget β . However, we have to find the optimal values for k and γ given

budget β . To do so, a naive solution would be to use full expansions (by setting $\gamma = 1$). Intuitively, this approach appears as suboptimal as it does not take into account the discrepancies between channel-wise quantization errors. Furthermore, we demonstrate that the higher K (the lower γ), the better:

Lemma 3. *Let f be a layer of real-valued weights W with a symmetric distribution. Then, for $K' < K$ two integers, we have:*

$$\text{Err} \left(R^{(1)} + \sum_{k=2}^{K'} R_{\gamma_1}^{(k)} \right) \geq \text{Err} \left(R^{(1)} + \sum_{k=2}^K R_{\gamma_2}^{(k)} \right) \quad (8)$$

where Err is the quantization error (i.e. the absolute difference between the quantized and original weights, as in Equation 4) and $K'\gamma_1 = K\gamma_2 = \beta$.

The proof is provided in Appendix B.3. This result motivates the use of high ordered, sparse, residual expansions. See Appendix D for a discussion on the value of K . In what follows, we show how developed networks can be approximated by equivalent ensembles of quantized DNNs for improved parallelization and acceleration.

3.3 Ensemble Expansion

Lemma 1 and 2 state that the first terms in the expansion, i.e. the lower values of k , are preponderant within the pre-activation term. Moreover, the activation functions traditionally used in DNNs (e.g. ReLU) satisfy $\sigma(x + \epsilon) \approx \sigma(x) + \sigma(\epsilon)$ when $|\epsilon| \rightarrow 0$. With respect to the proposed expansion, x corresponds to the first orders and ϵ to the terms of higher orders. In the case of two-layers networks, these properties allow us to break down the network in an (approximately) equivalent ensemble of two networks, the first one containing the first, largest orders, and the second one containing the remaining orders. Similarly, we demonstrate by structural induction (see Appendix E) that a network with arbitrary number of layers L can be approximated by an ensemble expansion $\tilde{f}^{(K)}$ composed of M quantized networks, defined by the parameters K_1, \dots, K_M setting the size of each predictor, such that $K_1 + \dots + K_M = K$ (the total number of orders in the expansion). Every predictor share the same architecture up to their respective expansion order. For each $m = 1, \dots, M$, the m^{th} predictor corresponds to the residuals at orders $k \in \{\sum_{l=1}^{m-1} K_l + i | i \in \{1, \dots, K_m\}\}$. This ensemble approximation allows to more efficiently parallelize the computations across the expansion orders for improved runtimes. It induces an error on the predictive function that can be bounded:

Lemma 4. *Let f be a L layers feed-forward DNN with ReLU activation $\sigma_{L-1} = \dots = \sigma_1$. The expected error $\mathbb{E} [\|f^{(K)} - \tilde{f}^{(K)}\|]$ due to the ensemble expansion of order K with M predictors, is bounded by U which can be approximated as:*

$$U \approx \frac{\sum_{k=1}^K \|R_L^{(k)}\|}{2^{L-1}} \sum_{m=1}^{M-1} \prod_{l=1}^{L-1} \sum_{k=K_m}^{K_{m+1}} \|R_L^{(k)}\| \lambda_{\tilde{h}_l}^{(k)} \quad (9)$$

We provide the elements of proof as well as the exact definition of U in Appendix B.4. To sum it up, any deep neural network can be approximated by an ensemble expansion of quantized networks, with theoretical guarantees of the approximation error. The method for computing the weights of the ensemble predictors is summarized in Algorithm 1. In practice, as we will showcase in the experiments, this ensemble approximation from expansion of residual errors leads to superior performances in term of accuracy-inference time trade-off.

4 Experiments

We validate the proposed method on three challenging computer vision tasks which are commonly used for comparison of quantization methods. First, we evaluate on ImageNet [12] ($\approx 1.2\text{M}$ images train/50k test) classification. Second, we report results on object detection on Pascal VOC 2012 [14] ($\approx 17\text{k}$ images in the test set). Third, we benchmark on image segmentation on CityScapes dataset [10] (500 validation images).

Algorithm 1 Ensemble Expansion Algorithm

Require: trained DNN f with L layers, hyper-parameters : K_1, \dots, K_M and γ such that $K = K_1 + \dots + K_M = K$ and the budget $\beta = (K - 1)\gamma$, operator Q

initialize γ^l ▷ equation 5

for $m \in \{1, \dots, M\}$ **do**

 initialize $f_m^{(K_m)}$ as a clone of f with K_m kernels per layer

end for

for $l \in \{1, \dots, L\}$ **do**

$W \leftarrow$ base kernel of layer l in f

$W_{\text{acc}} \leftarrow 0$ accumulated quantization error

for $m \in \{1, \dots, M\}$ **do**

for $k \in \{1, \dots, K_m\}$ **do**

$R_{\gamma^l}^{(k)} \leftarrow Q(W - W_{\text{acc}}) \mathbb{1}_{\gamma}^{(k)}$ ▷ equation 6

 set k^{th} kernel of layer l of $f_m^{(K_m)}$ with $R_{\gamma^l}^{(k)}$

$W_{\text{acc}} \leftarrow W_{\text{acc}} + Q^{-1}(R_{\gamma^l}^{(k)})$

end for

end for

end for

define $\tilde{f}^{(K)}$ as the sum of the $f_m^{(K)}$

In our experiments we used MobileNets [33] and ResNets [19] on ImageNet. For Pascal VOC object detection we employed an SSD [25] architecture with MobileNet backbone. On CityScapes we used DeepLab V3+ [6] with MobileNet backbone.

The implementation details are in Appendix F. In our experiments, the inputs and activations are quantized using the same method as in [29]. The number of bit-wise operation in our evaluation metric is discussed in Appendix G.

The experiments are divided in three sections. First, we validate the theoretical results as well as the practical added value of each step of REx on ImageNet classification. Second, we compare REx to other data-free quantization schemes including methods that generate synthetic data. Third, we generalize the previous results to other computer tasks, namely: semantic segmentation and object detection.

4.1 REx Empirical Validation

Expansion Validation: Fig 3 illustrates the trade-off between the accuracy on ImageNet of a ResNet 50 and a MobileNet v2 and the number of bit-wise operations. We report different expansion orders K (no sparsity) and number of bits b for standard bit representations ($b \geq 3$). In most cases, we observe a systematic convergence to the full-precision accuracy with $K = 2$. It is only for MobileNet with $b = 4$ that the setting $K \geq 3$ becomes mandatory to reach the full precision. This is an empirical validation of the exponential convergence w.r.t. the expansion order, as stated in lemma 1.

One more challenging benchmark for quantization methods is ternary quantization (TNN), where the quantized weights can either take the values $-1, 0$ or 1 . In such a case, higher values of K are required in order to reach the full-precision accuracy. This is also illustrated on Fig 3. Here again, the ternary-quantized models reach the full precision With $K = 5, 6$ for ResNet 50 and MobileNet v2 respectively. However, while this setting already constitutes a good trade-off between accuracy and number of bit-wise operations, using such high order expansions remains computationally expensive, without sparsity nor ensembling, as compared to a naive quantization scheme, *i.e.* using $K = 1$. This is addressed by budgeted sparsity and ensemble expansions.

Budgeted Expansion Validation: As stated in Lemma 3, given a specific budget, using higher order (high K) sparse (low γ) residual expansions allows to find a better accuracy vs. number of bit-wise operations trade-off. Intuitively, the lower b the bit width, the more fine-grained the possible budgets: therefore, REx performs better and is more flexible using low bit width such as ternary weights with sparse higher order expansions. For instance, on MobileNet, any values of $\beta = (K - 1)\gamma$

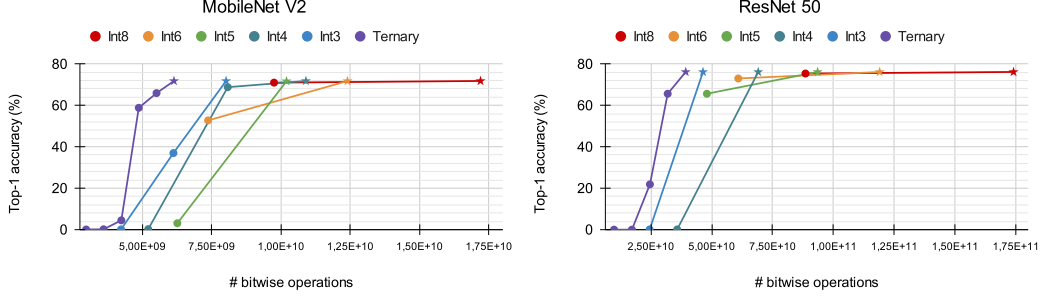


Figure 3: ImageNet top1 accuracy of quantized MobileNet V2 and ResNet 50. We compare the expansions at orders 1 – 3 for int3, int4, int5, int6 and int8 quantization as well as the ternary quantization of higher orders ($K = 5, 6$ respectively for ResNet 50 and MobileNet V2, in purple).

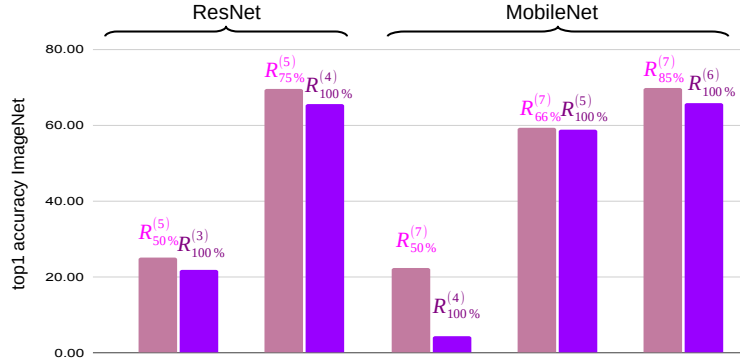


Figure 4: ImageNet top1 accuracy of MobileNet V2 and ResNet 50, and comparison between full expansions and sparse expansion of higher orders, with similar budgets for ternary quantization. In every case, the sparse expansion of higher orders achieves a better accuracy.

greater than 3 will reach the full-precision accuracy with int4 representations. Similarly, on ResNet, any value of β greater than 3.5 allows to reach the full-precision accuracy.

Fig 4 draws a comparison between full orders and sparse (higher) orders for an equivalent budget in case of ternary quantization: in every case, the sparse, high-order expansion achieves greater accuracy than the full, lower-order one: e.g. ResNet with $R_{75\%}^{(5)}$ achieves 69.53% top-1 accuracy vs 65.63% for $R_{100\%}^{(4)}$; MobileNet with $R_{85\%}^{(7)}$ achieves 69.88% top-1 accuracy vs 65.94% for $R_{100\%}^{(6)}$. We propose a more in-depth study of the behavior of the quantized neural networks w.r.t. extreme values of γ (below 0.1) in Appendix H. Overall, the budgeted expansion significantly improves the ternary quantization. It reduces by 15% and 20% the budget as compared to the standard expansion, in order to reach full-precision accuracy on ResNet 50 and MobileNet V2.

Ensemble Expansion Validation: Fig 5 showcases the normalized inference times on ImageNet of several ResNets and MobileNets, *i.e.* the inference time ratio between networks expansions (or ensemble expansions) at an arbitrary order vs the comparable baseline (order 1) network.

On the one hand, as indicated by the dashed plots (network expansions without ensembles), the relative inference time grows sublinearly for each networks, e.g. order 2 comes at virtually no cost in terms of inference time, while using higher orders induces a noticeable slow down ($< 50\%$ for order 3, $< 100\%$ at order 5).

On the other hand, when considering balanced ensembles, *i.e.* predictors with similar sizes (see Appendix I for a more detailed discussion), we observe that we can expand the quantized models up to order 4 without noticeably degrading the inference speed. This is due to more efficient parallelization of the ensembles compared to regular residual expansions, where, at inference time for each layer, all the residuals have to be computed so that the output of this layer can be provided as an input for the next layer. Furthermore, recall that using the ensemble expansion does fully preserve the

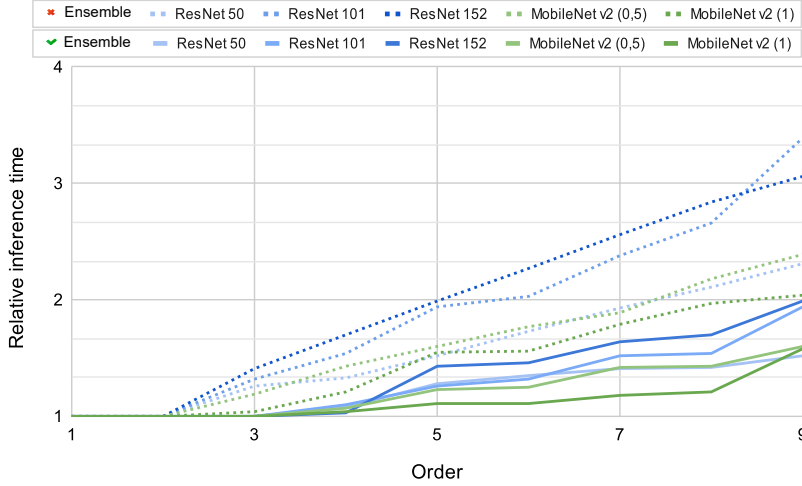


Figure 5: Standardized inference time on ImageNet of different architectures. We demonstrate that parallelization of the overhead computations drastically reduces their impact on runtime.

predictive function compared with the residual expansion (as theoretically justified in lemma 4 and empirically validated under certain assumptions, that are discussed in Appendix I). As a consequence, REx manages to achieve high efficiency by leveraging higher order residual expansions. Moreover, the group-sparse formulation allows to find better trade-off in terms of accuracy *vs.* the number of bit-wise operations. Last but not least, the proposed ensemble expansion allows to use high orders expansions without significantly impacting the inference time thanks to improved parallelization. In what follows we show that REx significantly improves over current state-of-the-art data-free quantization techniques.

4.2 Comparison with existing approaches

In Table 1, We compare REx and the state-of-the-art data-free quantization methods OCS [42], DFQ [29], SQNR [28] and methods that involve synthetic data, such as ZeroQ [4], DSG [41], GDFQ [40] and MixMix [23]. We report results on int8 and int4 quantization: for the former case, we use order 2 residual expansion without ensembling (as the inference time are equivalent with the baseline model, see Fig 5). For int4 quantization, we report results at order 4 with an ensemble of 2 predictors, each containing two orders, *i.e.* $K_1 = K_2 = 2$. Using this setup ensures that the inference runtimes are comparable (see Fig 5).

First, given a budget of bit-wise operations that achieves equivalent expected run-time (Fig 5), REx can achieve higher accuracy than existing approaches: e.g. on both MobileNet V2 and ResNet, in int4, REx outperforms SQuant [9], the best data-free method that does not involve data-generation (DG), by 16.3 points and 7.5 respectively. Note that other methods such as OCS (also involving structural changes in the neural network architecture) considerably underperforms, especially on int4 where the accuracy drops to 0.1. REx, however, fully preserves the floating point accuracy.

Second, REx even outperforms the impressive (yet time consuming) data-generation (DG) based methods such as ZeroQ [4], DSG [41], GDFQ [40] and MixMix [23]. The difference is more noticeable on low bit quantization, e.g. $b = 4$. For instance, on MobileNet V2, GDFQ and MixMix achieve 51.30 and 65.38 accuracy, respectively. Nevertheless, REx improves the accuracy on this benchmark by 6.35% top-1 accuracy. Similarly, on ResNet-50, REx reaches accuracies very close to the full precision model (76.13), significantly outperforming its closest contender, MixMix (74.58).

Third, as shown on Table 2, in terms of quantization processing time, methods relying on data generation (DG) such as ZeroQ [4], DSG [41], GDFQ [40] and MixMix [23] are slow as they usually require many forward-backward passes to quantize a trained neural network. REx, on the other hand, is very fast in addition to being better at preserving the original model accuracy.

Table 1: Accuracy for MobileNet V2 and ResNet 50 on ImageNet. REx (with ensembling) achieves excellent accuracy for both standard and low-bit quantization, more-so using high-order sparse expansions, vastly outperforming previous state-of-the-art data-free quantization approaches such as OCS, DFQ, SQNR and SQuant, and even approaches that require fine-tuning as MixMix, ZeroQ, DSG and GDFQ.

(a) MobileNet V2				(b) ResNet 50			
method	no-DG	b	accuracy	method	no-DG	b	accuracy
baseline	-	-	71.80	baseline	-	-	76.15
OCS	✓	8	71.10	OCS	✓	8	75.70
DFQ	✓	8	70.92	DFQ	✓	8	76.00
SQNR	✓	8	71.2	SQNR	✓	8	75.90
ZeroQ	✗	8	71.61	ZeroQ	✗	8	75.89
GDFQ	✗	8	71.80	DSG	✗	8	75.87
REx (2)	✓	8	71.80	REx (2)	✓	8	76.15
DFQ	✓	4	0.10	OCS	✓	4	0.1
ZeroQ	✗	4	49.83	DSG	✗	4	23.10
GDFQ	✗	4	51.30	GDFQ	✗	4	55.65
SQuant	✓	4	55.38	SQuant	✓	4	68.60
MixMix	✗	4	65.38	MixMix	✗	4	74.58
REx (4)	✓	4	71.73	REx (4)	✓	4	76.13

Table 2: REx, MixMix, GDFQ and ZeroQ 4-bit quantization time in seconds. REx was quantized such that full-precision accuracy is reached.

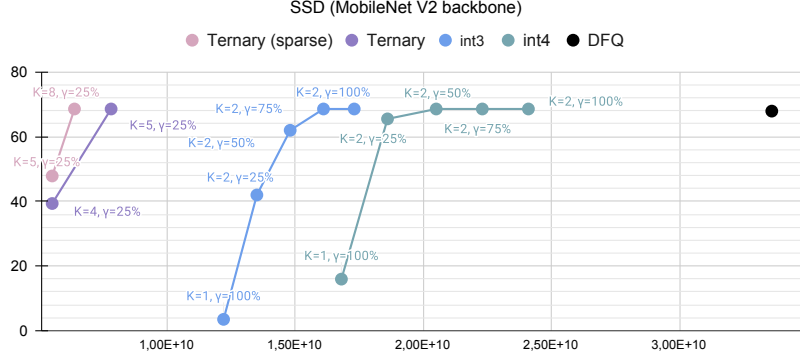
Model	ZeroQ	GDFQ	MixMix	REx
ResNet 50	92.1	11.10^3	18.10^3	<1
ResNet 101	164.0	18.10^3	25.10^3	<1
ResNet 152	246.4	24.10^3	30.10^3	1.1
MobileNet V2 (0.35)	27.4	3.10^3	6.10^3	<1
MobileNet V2 (1)	37.9	7.10^3	12.10^3	<1

4.3 Other Applications

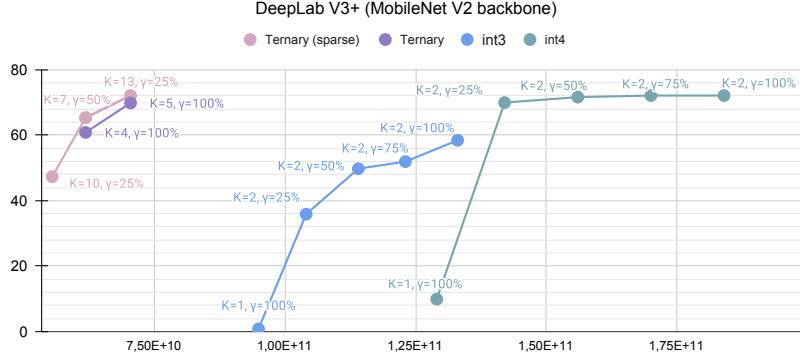
In this section, we show that REx is also very flexible and can be straightforwardly applied to other computer vision tasks, e.g. object detection and semantic segmentation.

Object Detection In Fig 6a, we report the performance of REx (as well as DFQ [29] for int8 quantization) using SSD-MobileNet as a base architecture for object detection. Overall, we observe a similar trend as in Section 4.2: REx reaches significantly lower numbers of bit-wise operations than the naive baseline ($R_{\gamma=100\%}^{k=1}$) and state-of-the-art DFQ [29] while preserving the full model accuracy, using either int4, int3 or ternary quantization. Also, once again, the best results are obtained using ternary quantization with high orders (e.g. $k = 8$) and sparse residuals (e.g. $\gamma = 25\%$): as such, the mAP of the best tested configuration, $R_{25\%}^{(8)}$, reaches 68.6% for $6.38e^9$ bit-wise operations, vs. 67.9% for $3.36e^{10}$ bit-wise operations for DFQ [29].

Semantic Segmentation In Fig 6b, we report the performance of REx for image segmentation using a DeepLab v3+ architecture. Similarly to the previous tasks, REx is able to very efficiently quantize a semantic segmentation network, whether it is in int4 or higher (where order 2 is sufficient to reach the full precision mIoU), or in int3/ternary quantization. In the latter case, once again, it is better to use sparse, high order expansions: for instance, we were able to retrieve the full accuracy using $R_{50\%}^{(9)}$ and ternary quantization, dividing by 10 the number of bit-wise operations as compared to the original model. This demonstrates the robustness of REx to the task and architecture.



(a)



(b)

Figure 6: (a) Mean average precision (mAP) of a SSD with MobileNet V2 backbone on Pascal VOC for object detection. We add the performance of a data-free quantization solution, DFQ [29] for comparison. (b) Mean intersection over union (mIoU) of a Deeplab V3+ with MobileNet V2 backbone on CityScapes for semantic segmentation.

5 Conclusion

In this work, we proposed a expansion of residual errors, dubbed REx, a novel data-free quantization method. We proposed to decompose the weights of each layer as an expansion of residual errors. Moreover, we designed a group-sparse budgeted version of REx, with exponential convergence towards the original weights. Lastly, expansions of quantized residual errors can be approximated by an equivalent ensemble of quantized DNNs that significantly increases the evaluation speed through more efficient parallelization, without accuracy loss. We provide strong theoretical and empirical evidence on the robustness of REx on several architectures, computer vision tasks, showing that REx dramatically outperforms state-of-the-art data-free quantization approaches.

Limitations: In this work, we use for each expansion order a naive per-layer, per-channel quantization. REx, however, is complementary to approaches that refine the quantization operator, e.g. DFQ [29], or the mixed precision methods [38, 7]. Thus, the results could in theory be improved by combining REx with these approaches. Furthermore, REx allows to significantly reduce the number of bit-wise operations of DNNs; the fact, however, that this eventually translate well in terms of inference time reduction may rely on specific, and potentially complex hardware-specific implementation.

References

- [1] Achterhold, J., Koehler, J.M., Schmeink, A., Genewein, T.: Variational network quantization. In: ICLR (2018)
- [2] Breiman, L.: Bagging predictors. *Machine learning* **24**(2), 123–140 (1996)
- [3] Breiman, L.: Arcing the edge. Tech. rep., Technical Report 486, Statistics Department, University of California at ... (1997)
- [4] Cai, Y., Yao, Z., Dong, Z., Gholami, A., Mahoney, M.W., Keutzer, K.: Zeroq: A novel zero shot quantization framework. In: CVPR. pp. 13169–13178 (2020)
- [5] Chen, L.C., Papandreou, G., Schroff, F., Adam, H.: Rethinking atrous convolution for semantic image segmentation. *arXiv preprint arXiv:1706.05587* (2017)
- [6] Chen, L.C., Zhu, Y., Papandreou, G., Schroff, F., Adam, H.: Encoder-decoder with atrous separable convolution for semantic image segmentation. In: ECCV. pp. 801–818 (2018)
- [7] Chen, W., Wang, P., Cheng, J.: Towards mixed-precision quantization of neural networks via constrained optimization. In: ICCV. pp. 5350–5359 (2021)
- [8] Chen, W., Wilson, J., et al.: Compressing neural networks with the hashing trick. In: ICML. pp. 2285–2294 (2015)
- [9] Cong, G., et al.: Squant: On-the-fly data-free quantization via diagonal hessian approximation. ICLR (2022)
- [10] Cordts, M., Omran, M., Ramos, S., Rehfeld, T., Enzweiler, M., Benenson, R., Franke, U., Roth, S., Schiele, B.: The cityscapes dataset for semantic urban scene understanding. In: CVPR. pp. 3213–3223 (2016)
- [11] Courbariaux, M., Hubara, I., et al.: Binarized neural networks: Training deep neural networks with weights and activations constrained to+ 1 or-1. *NeurIPS* (2016)
- [12] Deng, J., Dong, W., et al.: ImageNet: A Large-Scale Hierarchical Image Database. In: CVPR (2009)
- [13] Dietterich, T.G.: Ensemble methods in machine learning. In: International workshop on multiple classifier systems. pp. 1–15. Springer (2000)
- [14] Everingham, M., Van Gool, L., Williams, C.K.I., Winn, J., Zisserman, A.: The PASCAL Visual Object Classes Challenge 2012 (VOC2012) Results. <http://www.pascal-network.org/challenges/VOC/voc2012/workshop/index.html> (2012)
- [15] Friedman, J., Hastie, T., Tibshirani, R.: Additive logistic regression: a statistical view of boosting (with discussion and a rejoinder by the authors). *The annals of statistics* **28**(2), 337–407 (2000)
- [16] Gong, Y., Liu, L., Yang, M., Bourdev, L.: Compressing deep convolutional networks using vector quantization. *arXiv preprint arXiv:1412.6115* (2014)
- [17] Guo, J., Gould, S.: Deep cnn ensemble with data augmentation for object detection. *arXiv preprint arXiv:1506.07224* (2015)
- [18] Han, S., Mao, H., Dally, W.J.: Deep compression: Compressing deep neural networks with pruning, trained quantization and huffman coding. ICLR (2016)
- [19] He, K., Zhang, X., et al.: Deep residual learning for image recognition. In: CVPR. pp. 770–778 (2016)
- [20] Jacob, B., Kligys, S., Chen, B., Zhu, M., Tang, M., Howard, A., Adam, H., Kalenichenko, D.: Quantization and training of neural networks for efficient integer-arithmetic-only inference. In: CVPR. pp. 2704–2713 (2018)
- [21] Klarreich, E.: Multiplication hits the speed limit. *Communications of the ACM* **63**(1), 11–13 (2019)
- [22] Krishnamoorthi, R.: Quantizing deep convolutional networks for efficient inference: A whitepaper. *arXiv preprint arXiv:1806.08342* (2018)
- [23] Li, Y., Zhu, F., Gong, R., Shen, M., Dong, X., Yu, F., Lu, S., Gu, S.: Mixmix: All you need for data-free compression are feature and data mixing. In: ICCV. pp. 4410–4419 (2021)
- [24] Lin, D., Talathi, S., Annapureddy, S.: Fixed point quantization of deep convolutional networks. In: ICML. pp. 2849–2858. PMLR (2016)

- [25] Liu, W., Anguelov, D., Erhan, D., Szegedy, C., Reed, S., Fu, C.Y., Berg, A.C.: Ssd: Single shot multibox detector. In: ECCV. pp. 21–37. Springer (2016)
- [26] Louizos, C., Reisser, M., Blankevoort, T., Gavves, E., Welling, M.: Relaxed quantization for discretized neural networks. ICLR (2018)
- [27] Mallat, S.G.: A theory for multiresolution signal decomposition: the wavelet representation. In: Fundamental Papers in Wavelet Theory, pp. 494–513. Princeton University Press (2009)
- [28] Meller, E., Finkelstein, A., Almog, U., Grobman, M.: Same, same but different: Recovering neural network quantization error through weight factorization. In: ICML. pp. 4486–4495 (2019)
- [29] Nagel, M., Baalen, M.v., et al.: Data-free quantization through weight equalization and bias correction. In: ICCV. pp. 1325–1334 (2019)
- [30] Oh, S., Sim, H., Lee, S., Lee, J.: Automated log-scale quantization for low-cost deep neural networks. In: CVPR. pp. 742–751 (2021)
- [31] Rabbani, M.: Jpeg2000: Image compression fundamentals, standards and practice. *Journal of Electronic Imaging* **11**(2), 286 (2002)
- [32] Rame, A., Cord, M.: Dice: Diversity in deep ensembles via conditional redundancy adversarial estimation. ICLR (2021)
- [33] Sandler, M., Howard, A., et al.: Mobilenetv2: Inverted residuals and linear bottlenecks. In: CVPR. pp. 4510–4520 (2018)
- [34] Sheng, T., Feng, C., Zhuo, S., Zhang, X., Shen, L., Aleksic, M.: A quantization-friendly separable convolution for mobilenets. In: 2018 1st Workshop on Energy Efficient Machine Learning and Cognitive Computing for Embedded Applications (EMC2). pp. 14–18. IEEE (2018)
- [35] Stock, P., Graham, B., Gribonval, R., Jégou, H.: Equi-normalization of neural networks. ICLR (2019)
- [36] Tan, T.Y., Zhang, L., Lim, C.P., Fielding, B., Yu, Y., Anderson, E.: Evolving ensemble models for image segmentation using enhanced particle swarm optimization. *IEEE access* **7**, 34004–34019 (2019)
- [37] Ullrich, K., Meeds, E., Welling, M.: Soft weight-sharing for neural network compression. ICLR (2017)
- [38] Wang, K., Liu, Z., et al.: Haq: Hardware-aware automated quantization with mixed precision. In: CVPR. pp. 8612–8620 (2019)
- [39] Wu, S., Li, G., Chen, F., Shi, L.: Training and inference with integers in deep neural networks. ICLR (2018)
- [40] Xu, S., Li, H., Zhuang, B., Liu, J., Cao, J., Liang, C., Tan, M.: Generative low-bitwidth data free quantization. In: ECCV. pp. 1–17. Springer (2020)
- [41] Zhang, X., Qin, H., Ding, Y., Gong, R., Yan, Q., Tao, R., Li, Y., Yu, F., Liu, X.: Diversifying sample generation for accurate data-free quantization. In: CVPR. pp. 15658–15667 (2021)
- [42] Zhao, R., Hu, Y., Dotzel, J., De Sa, C., Zhang, Z.: Improving neural network quantization without retraining using outlier channel splitting. In: ICML. pp. 7543–7552 (2019)
- [43] Zhou, A., Yao, A., Guo, Y., Xu, L., Chen, Y.: Incremental network quantization: Towards lossless cnns with low-precision weights. ICLR (2017)
- [44] Zhou, S., Wu, Y., Ni, Z., Zhou, X., Wen, H., Zou, Y.: Dorefa-net: Training low bitwidth convolutional neural networks with low bitwidth gradients. *arXiv preprint arXiv:1606.06160* (2016)
- [45] Zhu, S., Dong, X., Su, H.: Binary ensemble neural network: More bits per network or more networks per bit? In: CVPR. pp. 4923–4932 (2019)

Table 3: Summary of notations

	symbol	meaning
parameters	b	number of bits for weights and activations representation
	β	budget of added computations
	K	maximum expansion order
	γ	sparsity parameter over the whole DNN
	γ^l	sparsity parameter for layer l
	M	number of predictors in the ensemble
DNN	f	full-precision DNN
	$f^{(k)}$	expansion at order k of f
	$\tilde{f}^{(k)}$	ensemble expansion of order k of f
Layer	f_l	full-precision layer l
	$f_l^{(k)}$	expansion at order k of layer l
	$\tilde{f}_l^{(k)}$	ensemble expansion at order k of layer l
Weights	W	full-precision weight tensor of a Layer
	$(W)_i$	Column i of W
	w	full-precision weight scalar
	$R^{(k)}$	weights of expansion of order k
	$w^{(k)}$	scalar weight values of $R^{(k)}$
	$R_\gamma^{(k)}$	sparse $R^{(k)}$ of budget γ
Scaling	$(\lambda)_i$	rescaling factor for column i
	$(\lambda_R^{(k)})_i$	rescaling factor of $R^{(k)}$ and column i
	$\lambda_{R_l^{(k)}}$	rescaling factor of $R^{(k)}$ and layer l
	$\lambda_{f_l^{(k)}}$	rescaling factor of $f_l^{(k)}$
	λ_x	rescaling factor of an input x
	x	input of the DNN
Inputs	X	input of the DNN
	$X_{f_{L-1}^{(k)}}$	transformation of x into the input of $f_{L-1}^{(k)}$
	$X_{g_{L-1}^{(k)}}$	transformation of x into the input of $g_{L-1}^{(k)}$
	$X_{h_{L-1}^{(k)}}$	transformation of x into the input of $h_{L-1}^{(k)}$

A Notations

We sum up our notations in Table 3. Our method has three hyper-parameters: the budget β , the highest expansion order K and m the number of predictors in the ensemble. These hyper-parameters define the maximum number of over-head computations allowed. Then we deduce the values of γ and γ^l to fit in the budget. Other notations are used in our lemma 1, 2, 3, 4 and 5 and corollary 1 and 2.

B Demonstrations

In this Appendix section we provide justifications to the lemma of the main paper.

B.1 Proof of Lemma 1: Convergence of the Expansion

Before detailing the proof of lemma 1, we empirically motivate the assumption of symmetry over the weigh values distribution. In Figure 7, we plot the distributions of the weights of several layers of a ResNet 50 trained on ImageNet. The assumption is clearly satisfied in practice.

Proof. Assume $K = 1$, then $W^{(1)}$ is the result of the composition of inverse quantization operator and quantization operator, i.e. $W^{(1)} = \lambda \lfloor \frac{W}{\lambda} \rfloor$. By definition of the rounding operator we know that $|\lfloor a \rfloor - a| \leq 0.5$. Thus we have $|w - w^{(1)}| \leq \lambda/2$. Now in the case $k = 2$, we have by definition of the quantization of the residual error and the property of the rounding operator

$$\left| \left\lfloor \frac{w - w^{(1)}}{\lambda^{(2)}} \right\rfloor - \frac{w - w^{(1)}}{\lambda^{(2)}} \right| \leq \frac{1}{2} \quad (10)$$

where $\lambda^{(2)}$ is the rescaling factor in the second order residual R^2 computed from $w - w^{(1)}$. The quantized weights are thus given by:

$$\left| w - \sum_{i=1}^2 w^{(i)} \right| \leq \frac{\lambda^{(2)}}{2} \quad (11)$$

Because the weight distribution is symmetric we know that for any k , $\lambda^{(K)} = \frac{\max\{w - \sum_{k=1}^{K-1} w^{(k)}\}}{2^{b-1}-1}$. Also, by definition we have $\max\{w - \sum_{k=1}^{K-1} w^{(k)}\} \leq \lambda^{(K-1)}$. Thus:

$$\left| w - \sum_{k=1}^2 w^{(k)} \right| \leq \left(\frac{1}{2^{b-1}-1} \right) \frac{\lambda}{2} \quad (12)$$

We conclude by using a trivial induction proof. \square

As an immediate consequence we have the following corollary which justifies the expansion appellation:

Corollary 1. *Let f be a layer of real-valued weights W with a symmetric distribution and $R^{(k)}$ the k^{th} quantized weight from the corresponding residual error. Then,*

$$\mathbb{E} \left[\left\| f - \sum_{k=1}^K f^{(k)} \right\| \right] \geq \mathbb{E} \left[\left\| f - \sum_{k=1}^{K+1} f^{(k)} \right\| \right] \quad (13)$$

and $f = \sum_{k=1}^{\infty} f^{(k)}$.

The first inequality results from detailing the induction in the previous proof. Instead of an upper bound on the error over all the scalar values we consider each error and show using the same properties that they go down after each step. $f = \sum_{k=1}^{\infty} f^{(k)}$ is a direct consequence of equation 4.

B.2 Proof of Lemma 2: Convergence of Sparse Expansions

Proof. From equation 4, we have:

$$\left| w - \left(\sum_{k=1}^{K-1} w^{(k)} + Q^{-1} \left(R_1^{(K)} \right) \right) \right| \leq \frac{(\lambda_{R^{(K)}})_i}{2} \left(\frac{1}{2^{b-1}-1} \right)^K \quad (14)$$

which corresponds to the case where $\gamma^l = 1$. If $\gamma^l < 1$, we have two possibilities for w . First, the coordinate in $N^{(K)}$ associated to is greater than $\tau_{\gamma^l}^{(K)}$ then we fall in the case where $R_{\gamma}^{(K)} = R^{(K)}$ and as such we have the result from equation 4 which is stronger than equation 7. Second, the coordinate in $N^{(K)}$ associated to is lower than $\tau_{\gamma^l}^{(K)}$. Then we have that the difference between the baseline weight w and the slim expansion is bounded by the expansion of lower order and the maximum of the norm $N^{(K)}$ which leads to the result in equation 7. \square

Empirical validation: In lemma 1 and 2 we stated the exponential convergence to 0 of the approximation error on the weight values. In order to empirically confirm this theoretical result, we quantize a ResNet 50 trained on ImageNet in ternary values for different orders K . As can be seen in Figure 8, the average error per layer, exponentially converges to 0 which matches our expectations. The figure also confirms the empirical result on the strategies for γ . The higher errors are located on the last layers, thus these layers require more attention.

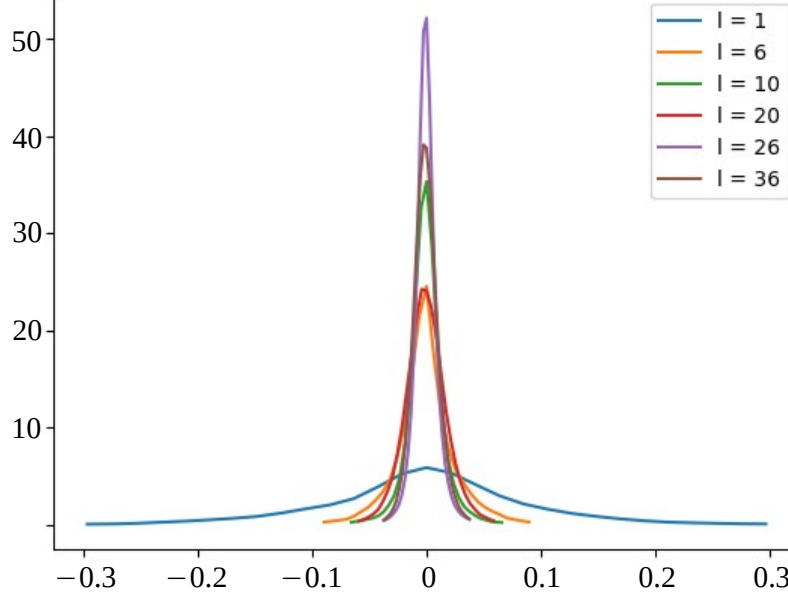


Figure 7: Distribution of the scalar weight values of different layers of a ResNet 50 trained on ImageNet. We observe that every distribution is symmetric around 0.

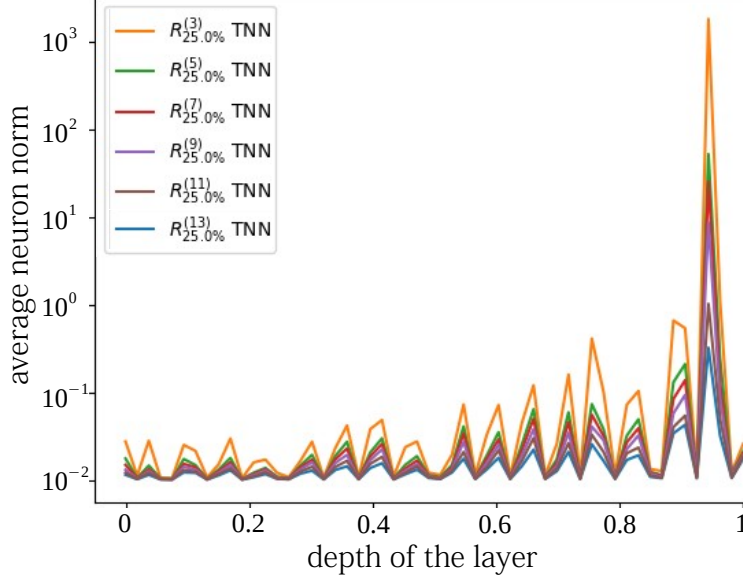


Figure 8: Comparison of the average norm of the quantization error for each layers of a ResNet 50 trained on ImageNet. We observe the exponential convergence stated in lemma 1 and 2.

B.3 Proof of Lemma 3: Higher Order and More Sparsity

Proof. Let's assume the layers outputs two channels. Then, we have $\gamma_1 = 1$ and $\gamma_2 = 0.5$. We simply need to prove the result for $k_1 = 2$ and $k_2 = 1$ as the result will extend naturally from this case. The idea of the proof consist in showing that using lower β values enables more possibilities of expansions which may lead to better performance. Let's note $(W)_1$ and $(W)_2$ the weights corresponding to the computation of the first and second output channels respectively. Using $\gamma_1 = 1$, the second order expansion correspond to either quantizing $(W)_1$ or $(W)_2$. Assume $(W)_1$ is chosen for $R_{\gamma_1}^{(2)}$. Then, $R_{\gamma_1}^{(3)}$ will either quantize the error from $(W)_2$ or further quantizes the error

from $R_{\gamma_1}^{(2)}$. In the first case we end up with $R^{(1)} + \sum_{i=2}^{k_1} R_{\gamma_1}^{(i)} = R^{(1)} + \sum_{n=2}^{k_2} R_{\gamma_2}^{(i)}$. Otherwise, $\text{Err} \left(R^{(1)} + \sum_{i=2}^{k_1} R_{\gamma_1}^{(i)} \right) > \text{Err} \left(R^{(1)} + \sum_{i=2}^{k_2} R_{\gamma_2}^{(i)} \right)$. \square

B.4 Proof of Lemma 4: Ensemble Expansion

Ensemble of two Layers DNNs Let f be a feed-forward DNN with two layers f_1, f_2 and σ a piece-wise affine activation function (e.g. ReLU). Given $(R_1^{(k)})_{k=1 \dots K}$ and b_1 the kernel and bias weights of the first layer $f_1^{(K)}$ respectively, we define the quantization expansion of residual errors $(R_1^{(k)})_{k \in \{1, \dots, K\}}$ of order K as in equation 3. Lemma 1 states that the first terms in the sum, i.e. the lower values of k , are preponderant in the pre-activation term. Thus, there exists $K_1 < K$ such that $f_1^{(K)} \approx \tilde{f}_1^{(K)} = \tilde{f}_{1,1}^{(K)} + \tilde{f}_{1,2}^{(K)}$ with:

$$\begin{cases} \tilde{f}_{1,1}^{(K)} : x \mapsto \sigma \left(\sum_{k=1}^{K_1} R_1^{(k)} x^q \lambda_{R_1^{(k)}} \lambda_x + b_1 \right) \\ \tilde{f}_{1,2}^{(K)} : x \mapsto \sum_{k=K_1+1}^K R_1^{(k)} x^q \lambda_{R_1^{(k)}} \lambda_x \end{cases} \quad (15)$$

Furthermore $f^{(K)} : x \mapsto f_2^{(K)}(f_1^{(K)}(x))$. Let $R_2^{(k)}$ and b_2 respectively denote the kernel and bias weights of the second layer $f_2^{(K)}$. By linearity of the last layer, we have

$$\begin{aligned} f^{(K)} \approx \tilde{f}^{(K)} &= \sum_{k=1}^K R_2^{(k)} \tilde{f}_{1,1}^{(K)} \lambda_{R_2^{(k)}} \lambda_{\tilde{f}_{1,1}^{(K)}} + b_2 \\ &+ \sum_{k=1}^K R_2^{(k)} \tilde{f}_{1,2}^{(K)} \lambda_{R_2^{(k)}} \lambda_{\tilde{f}_{1,2}^{(K)}} \end{aligned} \quad (16)$$

Stemming from this formulation, we can express the quantized network $f^{(K)}$ as an ensemble of quantized neural networks which share a similar architecture, i.e. $f^{(K)} \approx \tilde{f}^{(K)} = \tilde{g}^{(K)} + \tilde{h}^{(K)}$. This defines the ensemble expansion from residual errors of order K .

We provide the following intermediate result regarding two-layers DNNs.

Lemma 5. *Let f be a two layers feed-forward DNN with activation function $\sigma = \text{ReLU}$. The expected error $\mathbb{E} \left[\left\| f^{(K)} - \tilde{f}^{(K)} \right\| \right]$ due to the ensemble expansion of order K is bounded by U defined as:*

$$\begin{aligned} U &= \sum_{k=1}^K \left(1 - \mathbb{P} \left(f_1^{(K)} > 0 \cup \tilde{f}_{1,1}^{(K)} > 0 \right) \right) \lambda_{\tilde{f}_{1,2}^{(K)}} \lambda_{R_2^{(k)}} \| R_2^{(k)} \| \\ &\times \mathbb{E} \left[\left\| \tilde{f}_{1,2}^{(K)} \right\| \right] \end{aligned} \quad (17)$$

where $\|W\|$, for any set of weights W , denotes the norm operator or equivalently the spectral norm.

Proof. By definition of the ReLU activation function, if we have $f_1^{(K)} > 0$ then the activation function of f_1 behaves as the identity function. Similarly, if $\tilde{f}_{1,1}^{(K)} > 0$ then the activation function of \tilde{f}_1 also behaves as the identity. Therefore, if we have $(f_1^{(K)} > 0) \cup (\tilde{f}_{1,1}^{(K)} > 0)$, then $\tilde{f}_1^{(K)} = f_1^{(K)}$.

We deduce that $\mathbb{E} \left[\left\| f^{(K)} - \tilde{f}^{(K)} \right\| \right]$ is equal to

$$\int_{\{f_1^{(K)} > 0 \cup \tilde{f}_{1,1}^{(K)} > 0\}^C} \left\| f^{(K)}(x) - \tilde{f}^{(K)}(x) \right\| \mathbb{P} dx \quad (18)$$

where A^C the complementary set of a set A and x is the input. In the set defined by $\tilde{f}_{1,1}^{(K)}(x) = 0$, the value of $\tilde{f}_1^{(K)}(x)$ is the value of $\tilde{f}_{1,2}^{(K)}(x)$. If we also have $f_1^{(K)}(x) = 0$ then $\|f^{(K)}(x) - \tilde{f}^{(K)}(x)\| = \|\tilde{f}_{1,2}^{(K)}(x)\|$. We can deduce

$$\mathbb{E} \left[\left\| f_1^{(K)} - \tilde{f}_1^{(K)} \right\| \right] = \left(1 - \mathbb{P} \left(f_1^{(K)} > 0 \cup \tilde{f}_{1,1}^{(K)} > 0 \right) \right) \mathbb{E} \left[\left\| \tilde{f}_{1,2}^{(K)} \right\| \right] \quad (19)$$

The final result comes from the definition of the norm operator of a matrix and equation 16. \square

An immediate limit to lemma 5 is the difficulty to compute $1 - \mathbb{P}(f_1^{(K)} > 0 \cup \tilde{f}_{1,1}^{(K)} > 0)$. However this value can be approached under the assumption that the distribution of the activations is symmetrical around 0. Such instances appear with batch normalization layers and result in $1 - \mathbb{P}(f_1^{(K)} > 0 \cup \tilde{f}_{1,1}^{(K)} > 0) \approx \frac{1}{2}$. We also propose to compute the operator norm instead of $\mathbb{E}[\|\tilde{f}_{1,2}^{(K)}\|]$ in order to remain data-free. In consequence, we derive the following corollary.

Corollary 2. *The previous upper bound U on the expected error due to the ensemble expansion can be approximated as follows*

$$U \approx \frac{1}{2} \sum_{k=1}^K \|R_2^{(k)}\| \lambda_{\tilde{f}_{1,2}^{(K)}} \lambda_{R_2^{(k)}} \sum_{k=K_1}^K \|R_1^{(k)}\| \lambda_x \lambda_{R_1^{(k)}} \quad (20)$$

In practice, for expansion in b bits, with high values of b (e.g. $b \geq 4$), the single operator $R^{(1)}$ is enough to satisfy equation 15 and $K_1 = 1$. For lower values of b (e.g. ternary quantization), the suitable value for K_1 depends on the DNN architecture, usually ranging from 3 to 6.

Ensembling with more Layers We generalize this result to any feed-forward neural network f with $L > 2$ layers and activation functions $\sigma_1, \dots, \sigma_{L-1}$. Equation 3 becomes:

$$f_L^{(K)}(X_{f_{L-1}^{(K)}}) = \sum_{k=1}^K R_L^{(k)} X_{f_{L-1}^{(K)}} \lambda_{R_L^{(k)}} \lambda_{X_{f_{L-1}^{(K)}}} + b_L \quad (21)$$

where $X_{f_{L-1}^{(K)}} = f_{L-1}^{(K)} \circ \dots \circ f_1^{(K)}(x)$. We reason by induction on the layer $L - 1$. Similarly to what precedes, we assume that we have $\tilde{g}_{L-2}^{(K)}, \dots, \tilde{g}_1^{(K)}$ and $\tilde{h}_{L-2}^{(K)}, \dots, \tilde{h}_1^{(K)}$ such that:

$$f_{L-2}^{(K)} \circ \dots \circ f_1^{(K)}(x) \approx \tilde{g}_{L-2}^{(K)} \circ \dots \circ \tilde{g}_1^{(K)}(x) + \tilde{h}_{L-2}^{(K)} \circ \dots \circ \tilde{h}_1^{(K)}(x) \quad (22)$$

In order to simplify the composition notations, we note $X_{\tilde{f}}$ the input of a function \tilde{f} . With this in mind Eq. 16 becomes:

$$\left\{ \begin{array}{l} \tilde{f}^{(K)}(x) \approx \sum_{k=1}^K R_L^{(k)} \tilde{f}_{L-1}^{(K)}(x) \lambda_{R_L^{(k)}} \lambda_{\tilde{f}_{L-1}^{(K)}} + b_L \\ \tilde{f}_{L-1}^{(K)}(x) = \tilde{g}_{L-1}^{(K)}(X_{\tilde{g}_{L-1}^{(K)}}) + \tilde{h}_{L-1}^{(K)}(X_{\tilde{h}_{L-1}^{(K)}}) \\ \tilde{g}_{L-1}^{(K)}(X_{\tilde{g}_{L-1}^{(K)}}) = \sigma_{L-1} \left(\sum_{k=1}^{K_1} R_{L-1}^{(k)} \tilde{g}_{L-2}^{(K)}(X_{\tilde{g}_{L-2}^{(K)}}) \lambda_{R_{L-1}^{(k)}} \lambda_{\tilde{g}_{L-2}^{(K)}} + b_{L-1} \right) \\ \tilde{h}_{L-1}^{(K)}(X_{\tilde{h}_{L-1}^{(K)}}) = \sigma_{L-1} \left(\sum_{k=K_1+1}^K R_{L-1}^{(k)} \tilde{h}_{L-2}^{(K)}(X_{\tilde{h}_{L-2}^{(K)}}) \lambda_{R_{L-1}^{(k)}} \lambda_{\tilde{h}_{L-2}^{(K)}} \right) \\ X_{\tilde{g}_{L-1}^{(K)}} = \tilde{g}_{L-2}^{(K)} \circ \dots \circ \tilde{g}_1^{(K)}(x) \\ X_{\tilde{h}_{L-1}^{(K)}} = \tilde{h}_{L-2}^{(K)} \circ \dots \circ \tilde{h}_1^{(K)}(x) \end{array} \right. \quad (23)$$

The key element is the definition of $\tilde{g}_{L-1}^{(K)}$ and $\tilde{h}_{L-1}^{(K)}$, which are obtained by applying equation 16 two times, on $\tilde{g}_{L-2}^{(K)}$ and $\tilde{h}_{L-2}^{(K)}$ independently. This is detailed in Appendix E.

We showed that we can express $f^{(K)}$ as a sum of two quantized DNNs \tilde{g} and \tilde{h} . The first predictor \tilde{g} is equal to the expansion $f^{(K_1)}$ of f at order K_1 while \tilde{h} is equal to the expansion of $f^{(K)} - f^{(K_1)}$ at order $K - K_1$. This result can be extended to rewrite f as an ensemble of M predictors, by selecting K_1, \dots, K_M such that $\sum_{m=1}^M K_m = K$: in such a case, the M^{th} predictor will be the expansion of $f^{(K)} - f^{(\sum_{m=1}^{M-1} K_m)}$ at order K_M .

The proof of lemma 4 follows from lemma 5 and corollary 2. We derive the exact formula for the upper bound U in the general case of L layers feed forward neural networks

$$\sum_{k=1}^K \|R_L^{(k)}\| \prod_{l=1}^{L-1} \sum_{k=K_1}^K \mathbb{E}[\|\tilde{h}_l^{(k)}\|] \lambda_{\tilde{h}_l^{(k)}} P \quad (24)$$

Table 4: Top1 Accuracy of MobileNet V2 on ImageNet for a expansion in int6 and $R_{50\%}^{(2)}$. We tested each strategy and the linear ascending (linear+) is the best performing one.

	const	linear+	linear -	adaptive
MobileNet (0.35)	55.15	59.46	33.69	58.19
MobileNet (0.5)	51.59	64.96	46.56	64.43
MobileNet (0.75)	66.31	69.10	55.78	68.92
MobileNet (1)	67.07	71.55	56.98	70.85
MobileNet (1.4)	72.55	74.05	69.38	73.15

where $P = \left(1 - \mathbb{P}\left(f_l^{(K)} > 0 \cup \tilde{f}_l^{(K)} > 0\right)\right)$. This is a consequence of the definition of the operator norm and the proposed ensembling. The approximation is obtained under the same assumptions and with the same arguments as provided in Corollary 2.

C Choice of γ Strategy

We validate the strategy choice by trying four options of selection of the (γ^l) from γ and comparing the results on MobileNets for ImageNet. The candidates are:

1. the constant strategy where $\gamma^l = \gamma$ for all l
2. the proposed linear ascending strategy (noted linear ascending or linear+) from equation 5 which puts more importance on the last layers
3. the linear descending strategy (noted linear descending or linear-) which, on the contrary, puts more importance on the first layers
4. a width-adaptive strategy which is derived from the number of neurons/channels for each layer, such that $\gamma^l = \gamma \frac{L|W_l|}{\sum_l |W_l|}$

We tested the performance of the method with a budgetted expansion $R_{50\%}^{(2)}$ in int6 (with order $k = 2$ and $\gamma = 50\%$). The results are listed in Table 4. We observe that the linear+ strategy is the best performing one: one possible explanation is that the first layers of a DNN typically have fewer values, thus are easier to quantize well.

D On the limit value of K

In lemma 3, we stated, for a given budget β , the higher the value of K the lower the error. based on this result one may naively set γ to its lowest none-zero possible value, *i.e.* $\gamma = \frac{1}{|W|}$ where $|W|$ is the total number of weights in f . However, Table 5 we show that not only the error decreases when K increases but we also show its asymptotic behavior with a convergence for $K \approx 13 \pm 3$.

We want to put the emphasis on a counter intuitive aspect of our theoretical results. This asymptotic behavior is not a direct result of the exponential convergence demonstrated in lemma 1 and 2. In these lemmas, we show that for an increasing K and a similarly increasing budget the convergence to 0 is exponential. In lemma 3, we show that for a given budget the higher K the better. However, this is not enough to conclude that given a fixed β the convergence with respect to K is exponential to K . Furthermore depending on the budget β , in lemma 3 the limit is not necessarily 0. The empirical results from Table 5 demonstrate that in practice the convergence is also fast when the budget is fixed.

Table 5: Top1 accuracy on ImageNet for ternary quantization of ResNet 50 and MobileNet v2. We tested different depth N of expansion and the corresponding proportion γ in order to have a fixed budget β . The experimental results confirm Lemma 3.

Model	(N, γ)	β	accuracy
ResNet 50	(5, 50%)	2.5×10^{10}	16.55
ResNet 50	(9, 25%)	2.5×10^{10}	18.75
ResNet 50	(41, 5%)	2.5×10^{10}	20.05
ResNet 50	(4, 100%)	3.2×10^{10}	65.63
ResNet 50	(5, 75%)	3.2×10^{10}	69.53
ResNet 50	(13, 25%)	3.2×10^{10}	76.15
MobileNet v2	(7, 50%)	4.3×10^9	6.91
MobileNet v2	(30, 10%)	4.3×10^9	9.55
MobileNet v2	(60, 5%)	4.3×10^9	9.58
MobileNet v2	(5, 100%)	4.9×10^9	58.83
MobileNet v2	(9, 50%)	4.9×10^9	62.31
MobileNet v2	(41, 10%)	4.9×10^9	62.50

E Ensemble approximation of developed quantized DNNs

We recall that $f_{L-1}^{(K)}(x) = \sigma_{L-1} \left(\sum_{k=1}^K R_{L-1}^{(k)} \lambda_{R_{L-1}^{(k)}} X_{f_{L-1}^{(K)}} + b_{L-1} \right)$. If we directly apply equation 15 then we get for a given $K_{L-1} < K$

$$\begin{aligned}
 X_{f_{L-1}^{(K)}} \mapsto & \sigma_{L-1} \left(\sum_{k=1}^{K_{L-1}} R_{L-1}^{(k)} X_{f_{L-1}^{(K)}} \lambda_{X_{f_{L-1}^{(K)}}} \lambda_{R_{L-1}^{(k)}} + b_{L-1} \right) \\
 & + \sum_{k=K_{L-1}+1}^K R_{L-1}^{(k)} X_{f_{L-1}^{(K)}} \lambda_{X_{f_{L-1}^{(K)}}} \lambda_{R_{L-1}^{(k)}}
 \end{aligned} \tag{25}$$

However the two terms $X_{f_{L-1}^{(K)}}(x)$ inside and outside the activation function are not independent. Furthermore, the terms that compose $X_{f_{L-1}^{(K)}}(x)$, from equation 23, do not have the same range values, *i.e.* $\tilde{g}_{L-2}^{(K)}(X_{\tilde{g}_{L-2}^{(K)}}) \lambda_{\tilde{g}_{L-2}^{(K)}} >> \tilde{h}_{L-2}^{(K)}(X_{\tilde{h}_{L-2}^{(K)}}) \lambda_{\tilde{h}_{L-2}^{(K)}}$. We define the operation $*$ as follows

$$\begin{aligned}
 \tilde{f}_{L-1}^{(K)}(x) = & \sigma_{L-1} \left(\sum_{k=1}^{K_{L-1}} R_{L-1}^{(k)} \tilde{g}_{L-2}^{(K)}(X_{\tilde{g}_{L-2}^{(K)}}) \lambda_{R_{L-1}^{(k)}} \lambda_{\tilde{g}_{L-2}^{(K)}} + b_{L-1} \right) \\
 & + \sum_{k=K_{L-1}+1}^K R_{L-1}^{(k)} \tilde{g}_{L-2}^{(K)}(X_{\tilde{g}_{L-2}^{(K)}}) \lambda_{R_{L-1}^{(k)}} \lambda_{\tilde{g}_{L-2}^{(K)}} \\
 & + \sigma_{L-1} \left(\sum_{k=1}^{K_{L-1}} R_{L-1}^{(k)} \tilde{h}_{L-2}^{(K)}(X_{\tilde{h}_{L-2}^{(K)}}) \lambda_{R_{L-1}^{(k)}} \lambda_{\tilde{h}_{L-2}^{(K)}} \right) \\
 & + \sum_{k=K_{L-1}+1}^K R_{L-1}^{(k)} \tilde{h}_{L-2}^{(K)}(X_{\tilde{h}_{L-2}^{(K)}}) \lambda_{R_{L-1}^{(k)}} \lambda_{\tilde{h}_{L-2}^{(K)}}
 \end{aligned} \tag{26}$$

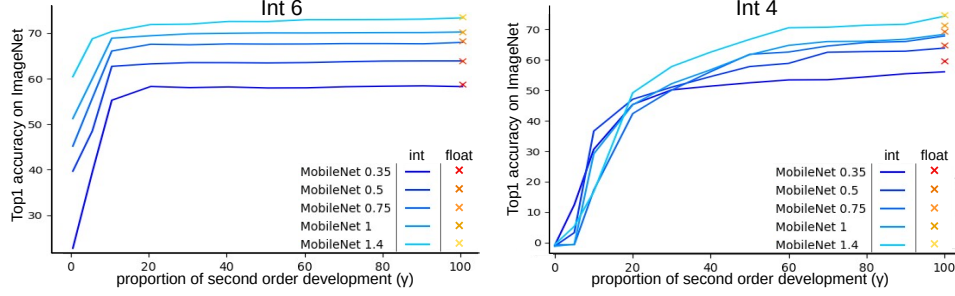


Figure 9: The top1 accuracy of MobileNets on ImageNet quantized in int6 (left) and int4 (right) as a function of γ for $k = 2$. We observe an immediate boost ($\gamma < 10\%$), especially in int6. Thus, the expansion can be used efficiently at a low overhead cost.

Table 6: Processing time on an Intel(R) Core(TM) i9-9900K CPU @ 3.60GHz of the proposed method for different configurations and architectures on ImageNet and a quantization in TNN. We note 'm' for minutes and 's' for seconds.

k	ensembling	ResNet 152	MobileNet v2 (1.4)
1	✗	0.32s	0.12s
2	✗	0.43s	0.13s
2	✓	0.43s	0.13s
7	✗	0.90s	0.51s
7	✓	0.92s	0.51s

Now, we have two independent functions $\tilde{g}_{L-1}^{(K)}$ and $\tilde{h}_{L-1}^{(K)}$ such that $\tilde{f}_{L-1}^{(K)} = \tilde{g}_{L-1}^{(K)} + \tilde{h}_{L-1}^{(K)}$, these functions have independent inputs and

$$\left\{ \begin{array}{l} \tilde{g}_{L-1}^{(K)}(X_{\tilde{g}_{L-2}^{(K)}}) = \sigma_{L-1} \left(\sum_{k=1}^{K_{L-1}} R_{L-1}^{(k)} \tilde{g}_{L-2}^{(K)}(X_{\tilde{g}_{L-2}^{(K)}}) \lambda_{R_{L-1}^{(k)}} \lambda_{\tilde{g}_{L-2}^{(K)}} + b_{L-1} \right) \\ \quad + \sum_{k=K_{L-1}+1}^K R_{L-1}^{(k)} \tilde{g}_{L-2}^{(K)}(X_{\tilde{g}_{L-2}^{(K)}}) \lambda_{R_{L-1}^{(k)}} \lambda_{\tilde{g}_{L-2}^{(K)}} \\ \tilde{h}_{L-1}^{(K)}(X_{\tilde{h}_{L-2}^{(K)}}) = \sigma_{L-1} \left(\sum_{k=1}^{K_{L-1}} R_{L-1}^{(k)} \tilde{h}_{L-2}^{(K)}(X_{\tilde{h}_{L-2}^{(K)}}) \lambda_{R_{L-1}^{(k)}} \lambda_{\tilde{h}_{L-2}^{(K)}} \right) \\ \quad + \sum_{k=K_{L-1}+1}^K R_{L-1}^{(k)} \tilde{h}_{L-2}^{(K)}(X_{\tilde{h}_{L-2}^{(K)}}) \lambda_{R_{L-1}^{(k)}} \lambda_{\tilde{h}_{L-2}^{(K)}} \end{array} \right. \quad (27)$$

This defines an iterative procedure in order to define our ensembling of expansions of residual errors for a feed-forward neural network f with any number L of layers.

To sum it up, the resulting predictors share an identical architecture up to their respective expansion order, defined by K_1 . The crucial difference comes from their weight values which correspond to different orders of expansion of the full-precision weights. This is also the case if we want ensembles of three or more predictors. In such instances, instead of only K_1 , we would have K_1, \dots, K_{m-1} for m predictors.

F Implementation Details

We used Tensorflow implementations of the baseline models from the official repository when possible or other publicly available resources when necessary. MobileNets and ResNets for ImageNet come from tensorflow models zoo. In object detection, we tested the SSD model with a MobileNet backbone from Manish's git repository. Finally, in image semantic segmentation, the DeepLab V3+ model came from Bonlime's git repository.

The networks pre-trained weights provide standard baseline accuracies on each tasks. The computations of the residues as well as the work performed on the weights were done using the Numpy python's library. As listed in Table 6, the creation of the quantized model takes less than a second for a MobileNet V2 as well as for a ResNet 152 without any optimization of the quantization process. These results were obtained using an Intel(R) Core(TM) i9-9900K CPU @ 3.60GHz.

G Operation Head-count

Let W be the real-valued weights of a $d \times d$ convolutional layer on input feature maps of shape $D \times D \times n_i$ and n_o outputs and stride s . Then the convolutional product requires $d^2 \frac{D^2}{s^2} n_i n_o$ floating point multiplications. The quantized layer requires two rescaling operations (for the quantization of the inputs and the Q^{-1} operation) and an int- b convolution, i.e. $n_i D^2 + \frac{D^2}{s^2} n_o$ floating point multiplications and $d^2 \frac{D^2}{s^2} n_i n_o$ int- b multiplications. Note that the number of additions remains unchanged. According to [21] the lowest complexity for b -digits scalar multiplication is $o(b \log(b))$ bit operations. This is theoretically achieved using Harvey-Hoeven algorithm (also the asymptomatic bound has yet to be proved). We use this value as it is the least favorable setup for the proposed method. As a consequence the number O_{original} bit operations required for the original layer, $O_{R^{(1)}}$ the number of bit operations for the naively quantized layer and $O_{R^{(k)}}$ for the i^{th} order residual quantization expansion are

$$\begin{cases} O_{\text{original}} = D^2 \frac{d^2 n_i n_o}{s^2} 32 \log(32) \\ O_{R^{(1)}} = D^2 \left[\left(n_i + \frac{n_o}{s^2} \right) 32 \log(32) + \frac{d^2 n_i n_o}{s^2} b \log(b) \right] \\ O_{R^{(k-1)}} = D^2 \left[\left(n_i + \frac{n_o}{s^2} \right) 32 \log(32) + k \frac{d^2 n_i n_o}{s^2} b \log(b) \right] \end{cases} \quad (28)$$

Using this result we can estimate the maximum order of expansion before which the number of operations in $f^{(k)}$ exceeds the O_{baseline} . Note that in the case of fully-connected layers, $D = 1$, $s = 1$ and $d = 1$. In the following section, we use the induced metric of accuracy with respect to the total number of bit-wise operations performed by the DNN on a single input. This metric doesn't consider the fact that the added operations can be performed in parallel.

H The Robustness to the Value of γ

the Performance boost due to the group-sparsity expansion is immediate, *i.e.* even for small values of γ . This can be seen in Figure 9, where we show for different bit widths (int6 and int4) the influence of γ on the accuracy of several MobileNet V2 architectures (with various width multipliers) on ImageNet. In int4, the accuracy reaches its asymptotic convergence for $\gamma \approx 50\%$ but large improvements are already made for values below 20%. This is even more impressive in int6 where the accuracy is restored with $\gamma \approx 25\%$ and a significant increase can be observed for values below 10%. Note that under 20% the computation overhead is negligible.

I How to set predictors size

We consider quantized expansions of networks with M predictors such that $\sum_{m=1}^M K_m = K$ (K_1 is the number of orders in the first predictor of the ensemble) and γ the sparsity factor. The larger K_1 , the lower the difference between the ensemble $\tilde{f}^{(K)}$ and the developed network $f^{(K)}$. Conversely, the more balanced the elements of the ensemble, the more runtime-efficient the ensemble: thus, K_1 have to be fixed carefully so that the ensemble shall be faster than the developed network, without accuracy loss. Fortunately, the accuracy behaviour w.r.t. the value of K_1 can be estimated from the values of the upper bound U (Lemma 4) on the expected error from ensembling $\mathbb{E}[\|f^{(K)} - \tilde{f}^{(K)}\|]$. As illustrated on Figure 10 in the case of ternary quantization, this upper bound is tight and collapses more than exponentially fast w.r.t. K_1 . For instance, if $K_1 \leq 2$, U is significantly larger than the amplitude of the logits $\mathbb{E}[\|f^{(K)}\|]$ and the accuracy is at risk of collapsing. When U vanishes compared to $\mathbb{E}[\|f^{(K)}\|]$, the ensemble and regular expansions are guaranteed to be almost identical, and the accuracy is preserved. Thus, we can compare the upper bound U and the empirical norm of the logits from the expansion $\mathbb{E}[\|f^{(K)}\|]$ to assess the validity of an ensemble. Plus, $\mathbb{E}[\|f^{(K)}\|]$ can be estimated using statistics from the last batch norm layers to allow for a fully data-free criterion.

With this in mind, in Figure 11 we compare the top-1 accuracies of $\tilde{f}^{(K)}$ and $f^{(K)}$ for different architectures (MobileNet v2 and ResNet 50) and quantization configurations. The ensemble expansion systematically matches the accuracy of the developed network in terms of accuracy, except in the case of ternary quantization when $K_1 = 1$. This is remarkable as ensembling significantly decreases the inference time with a two predictors configuration.

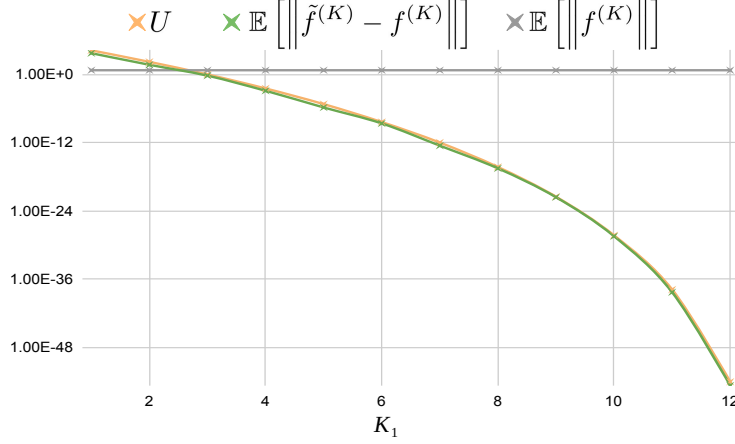


Figure 10: Comparison between the expected empirical error from ensembling $\mathbb{E}[\|f^{(K)} - \tilde{f}^{(K)}\|]$ (green) and its upper bound U (Lemma 4, orange) for different values of K_1 on a ResNet 50 trained on ImageNet and quantized with ternary values and $K = 13$, $\gamma = 25\%$. We also plot the reference $\mathbb{E}[\|f^{(K)}\|]$ (grey).

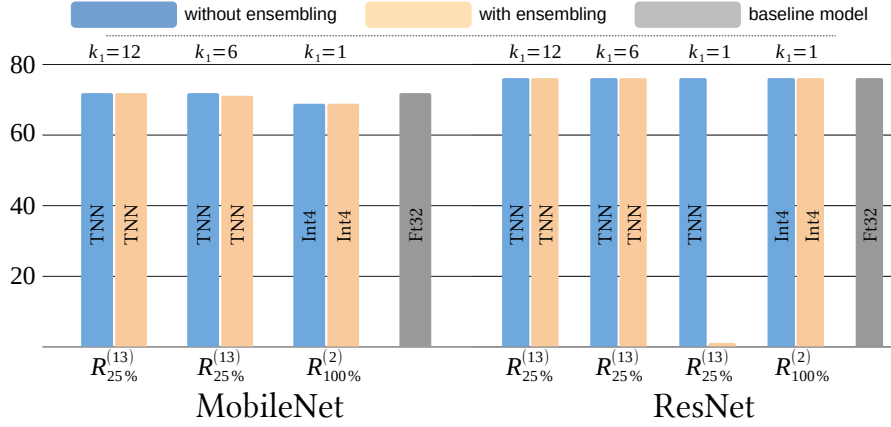


Figure 11: Comparison between ensemble expansion $\tilde{f}^{(K)}$ (in orange) and regular expansion $f^{(K)}$ (blue) on ImageNet. We test different bit representations, namely ternary (TNN) and int4 as well as different values for K_1 . Except for very low values the ratio K_1/K , we observe the robustness of the ensembling method.

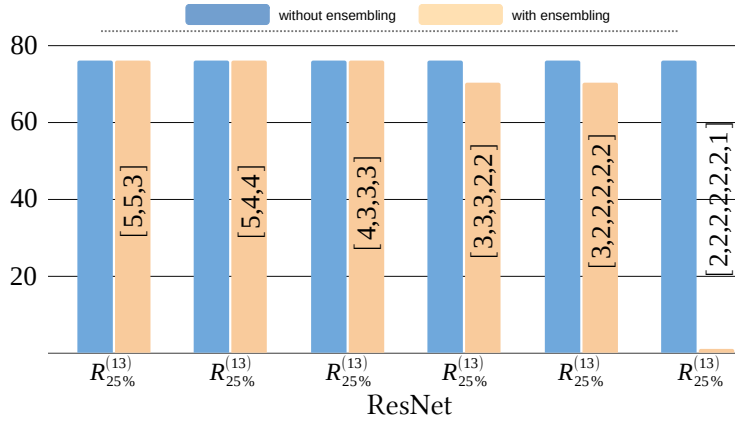


Figure 12: Comparison between TNN ensemble expansion $\tilde{f}^{(K)}$ (in orange) and regular expansion $f^{(K)}$ (blue) on ImageNet.

Table 7: Comparison of the evaluation time in seconds of a ResNet 50 over the validation set of ImageNet using a expansion of order $k = 8$ with ensembling of m predictors $m \in \{1, 2, 3, 4\}$. We distinguish the setups by reporting the values of $[K_1, \dots, K_m]$.

device	[8]	[4, 4]	[3, 3, 2]	[2, 2, 2, 2]	[1]
expansion	✓	✓	✓	✓	✗
ensembling	✗	✓	✓	✓	✗
Intel(R) i9-9900K	215	54	26	26	25
Ryzen 3960X	122	30	23	22	22
RTX 2070	13	8	5	5	5
RTX 3090	11	7	4	4	4

Figure 12 shows the results obtained with larger ensembles of smaller quantized predictors, *i.e.* with $M > 2$. We observe the full preservation of the accuracy of the developed network as long as $K_1 \geq 4$ and a loss of 6 points for balanced ensembles of 5 – 6 predictors and $K_1 = 3$. Here again, with $M = 7$ and $K_1 = 2$, the accuracy is very low, as predicted by 10. To sum it up, ensembling developed networks allows to significantly decrease the inference time, with theoretical guarantees on the accuracy preservation.

Finally, Table 7 shows the runtime of a ResNet 50 for a full evaluation on ImageNet validation set (50,000 images). We tested the models on different devices (CPU/GPU) using a fixed budget $\beta = 7$ and order $K = 8$, and compared ensembles expansions (with 2 [4, 4], 3 [3, 3, 2] and 4 [2, 2, 2, 2] predictors). On each device, the ensembles are up to 10 times faster than the baseline expansion.